

Document made available under the Patent Cooperation Treaty (PCT)

International application number: PCT/US05/002032

International filing date: 21 January 2005 (21.01.2005)

Document type: Certified copy of priority document

Document details: Country/Office: US
Number: 60/538,393
Filing date: 22 January 2004 (22.01.2004)

Date of receipt at the International Bureau: 03 March 2005 (03.03.2005)

Remark: Priority document submitted or transmitted to the International Bureau in compliance with Rule 17.1(a) or (b)



World Intellectual Property Organization (WIPO) - Geneva, Switzerland
Organisation Mondiale de la Propriété Intellectuelle (OMPI) - Genève, Suisse

1287409

THE UNITED STATES OF AMERICA

TO ALL TO WHOM THESE PRESENTS SHALL COME:

UNITED STATES DEPARTMENT OF COMMERCE

United States Patent and Trademark Office

February 18, 2005

THIS IS TO CERTIFY THAT ANNEXED HERETO IS A TRUE COPY FROM THE RECORDS OF THE UNITED STATES PATENT AND TRADEMARK OFFICE OF THOSE PAPERS OF THE BELOW IDENTIFIED PATENT APPLICATION THAT MET THE REQUIREMENTS TO BE GRANTED A FILING DATE.

APPLICATION NUMBER: 60/538,393

FILING DATE: *January 22, 2004*

RELATED PCT APPLICATION NUMBER: *PCT/US05/02032*



Certified by

Under Secretary of Commerce
for Intellectual Property
and Director of the United States
Patent and Trademark Office

PROVISIONAL APPLICATION FOR PATENT COVER SHEET

This is a request for filing a PROVISIONAL APPLICATION FOR PATENT under 37 CFR 1.53(c).

Express Mail Label No. EV311438025US

INVENTOR(S)		
Given Name(first and middle(if any))	Family Name or Surname	Residence (City and either State or Foreign Country)
William J.	Van Ooij	Fairfield, Ohio
<input checked="" type="checkbox"/> Additional inventors are being named on the <u>1</u> separately numbered sheets attached hereto.		

TITLE OF INVENTION (500 characters max)
ALLOY COMPOSITION FOR HOT-DIP GALVANIZING

Direct all correspondence to:

CORRESPONDENCE ADDRESS☐ Customer Number


26874

OR

<input checked="" type="checkbox"/> Firm or Individual Name	Stephen R. Albainy-Jenei, Frost Brown Todd LLC				
Address	2200 PNC Center				
Address	201 East Fifth Street				
City	Cincinnati	State	OH	ZIP	45202-4182

ENCLOSED APPLICATION PARTS (check all that apply)	
<input checked="" type="checkbox"/> Specification Number of Pages	25 <input type="checkbox"/> CD(s), Number
<input checked="" type="checkbox"/> Drawing(s) Number of Sheets	18 <input type="checkbox"/> Other (specify)
<input type="checkbox"/> Application Data Sheet. See 37 CFR 1.76	
METHOD FOR PAYMENT OF FILING FEES FOR THIS PROVISIONAL APPLICATION FOR PATENT	
<input checked="" type="checkbox"/> Applicant claims small entity status. See 37 CFR 1.27	FILING FEE Amount (\$) \$80.00
<input checked="" type="checkbox"/> A check is enclosed to cover the filing fees	
<input checked="" type="checkbox"/> The Director is hereby authorized to charge filing fees or credit any overpayment to Deposit Account 06-2226	
The invention was made by an agency of the United States Government or under a contract with an agency of the United States Government	
<input checked="" type="checkbox"/> No	
<input type="checkbox"/> Yes, the name of the U.S. Government agency and the Government contract number are:	

(Page 1 of 2)

Respectfully submitted,	Date <u>January 22, 2004</u>
SIGNATURE 	REGISTRATION NO. <u>41,487</u>
TYPED or PRINTED NAME <u>Stephen R. Albainy-Jenei</u>	Docket Number <u>91830.0521783</u>
TELEPHONE <u>513-651-6839</u>	

USE ONLY FOR FILING A PROVISIONAL APPLICATION FOR PATENT

SEND TO: Mail Stop Pr visional Applicati n, Commissioner for Patents, P.O. B x 1450, Alexandria, VA 22313-1450.

23026 U.S. PTO
01220422154 U.S. PTO
607538393
012204

PROVISIONAL APPLICATION FOR PATENT COVER SHEET
Additional Page

Docket Number 91830.0521783		
INVENTOR(S)/APPLICANT(S)		
Given Name(first and middle(if any))	Family Name or Surname	Residence (City and either State or Foreign Country)
Madhu	Ranjan	Cincinnati, Ohio
Ernest Edward	Klerks	Loveland, Ohio

[Page 2 of 2]

Number 2 of 2

U.S. PROVISIONAL PATENT APPLICATION

ALLOY COMPOSITION FOR HOT-DIP GALVANIZING

Inventors: William J. Van Ooij, Madhu Ranjan, Earnest Edward Klerks

Attorney Docket No.: 91830.0521783

**Stephen R. Albainy-Jenei
Registration No. 41,487
FROST BROWN TODD LLC
2200 PNC Center
201 East Fifth Street
Cincinnati, Ohio 45202
(513) 651-6839**

"Express Mail" mailing label number

EV311438025US

January 22, 2004

Date of Deposit

I hereby certify that this paper or fee is being deposited with the United States Postal Service "Express Mail Post Office to Addressee" service under 37 CFR §1.10 on the date indicated above and is addressed to Mail Stop: Provisional Patent Application, Commissioner for Patents, P.O. Box 1450, Alexandria, VA 22313-1450.

Matthew G. Burgan

(Type or print name of person mailing paper of fee)

Signature



ALLOY COMPOSITION FOR HOT-DIP GALVANIZING

Abstract

A zinc-aluminum eutectoid galvanized steel has been developed to address issues related to the growing environmental concern regarding leaching of zinc into the soil. The basic composition of the bath was selected close to the eutectoid point in the binary Zn-Al system, together with ternary additions in the form of bismuth, rare-earths and silicon. The effects of these additions on the growth rate, microstructure and corrosion properties of the coatings were investigated. Bismuth and rare-earths showed a minimal effect on controlling the coating thickness developed with the eutectoid bath composition, which was about an order thicker than commercially prevalent value of ~80µm. Addition of silicon to the bath reduced the thickness of the coating to a level of around 30 µm. The morphology of the coatings, investigated in detail using scanning electron microscopy, energy dispersive spectroscopy and x-ray diffraction, showed the presence of three layers: interface layer, intermediate layer and overlay. The dense interfacial layer mainly consisted of the Fe₂Al₅ phase, the intermediate layer contained two phases, an Fe-Al phase and a Zn-rich phase, and the overlay had a composition close to that of the liquid bath. The intermediate layer contained varying amount of porosity in all cases except in the coatings formed by the silicon containing bath. The thin, dense and smooth coating obtained with the latter bath showed excellent resistance to corrosion, evaluated by field exposure as well as by electrochemical tests. An attempt is made to unravel the role of different elements in the formation of coating microstructure.

1.0 Introduction

Improvement in corrosion resistance of steel products by coatings with zinc or its alloys is commonly known as galvanizing. Zinc provides corrosion resistance to steel by

barrier protection as well as by galvanic protection. Zinc is less noble than iron and is preferentially attacked, thus protecting the base metal. Hot-dip-galvanized (HDG) coatings are applied by dipping the steel component in the molten zinc or its alloys either in a continuous manner or by a batch process. The coatings from a zinc bath are very adherent to the base metal because of the formation of the metallic bond between the base metal and zinc. These coatings, in general, consist of an overlay and an interfacial layer between the overlay and the substrate steel. The interfacial layer contains a series of intermetallic compounds [1] which are brittle, and therefore detrimental to the formability of the coated steel.

In recent times there has been a growing environmental concern in Europe regarding leaching of zinc into the soil, which is likely to call for imposition of restrictions on the rate of leaching of zinc into the environment. The rate of leaching, which is a result of atmospheric corrosion and weathering, can be controlled if the coating has greater resistance to corrosion. Therefore, attempts are being made to produce a more corrosion-resistant coating by modifying the chemistry of the bath and by keeping a close control over the quality of the galvanized coating. Research has shown that addition of aluminum in varying amounts not only reduces the rate of leaching of zinc by providing an excellent barrier protection but also suppresses the formation and growth of the brittle iron-zinc intermetallic compounds. This is due to the formation of an inhibition layer [2] at the substrate/coating interface, which is an Fe-Al phase with limited solubility for Zn [3]. However, controlled growth of the Fe-Al based ternary intermetallics is very important not only for control over coating thickness but also to improve the appearance of the coated surface [4].

Inhibition of Fe-Zn reactions is known to be transient, since Al delays the Fe-Zn reaction rather than suppressing it completely, and eventually Fe-Zn outbursts form [5]. In order to delay the breakdown of the inhibition layer, and also to suppress the excess formation of the Fe-Al compounds, the high aluminum-containing zinc bath can be alloyed with ternary elements [6, 7]. Al provides very good barrier protection, and in combination with the excellent galvanic protection of Zn, galvanized products from Zn-Al baths such as Galfan® [8] and Galvalume® [9] provide corrosion protection several times better than that of Zn coatings [10].

Zinc alloys with 20-30 wt% Al are superplastic and continues to be under intensive investigation [11].

In the present study the influence of minor additions of Bi, rare-earth (RE) and Si to a Zn-22.3 wt% Al eutectoid bath on coating quality with respect to thickness, structure and corrosion properties has been studied. The main objectives of the research were:

- to identify the most suitable ternary addition to produce defect-free galvanic coating
- to investigate the role of various elements in the formation of the galvanic coating
- to determine the corrosion properties of the new product.

2.0 Experimental Procedures

Cold-rolled and annealed mild steel (Fe- 0.08 C, 0.32 Mn, 0.008 P, 0.013 S, 0.010 Si and 0.047 Al) sheets with dimension of 125x50x1.6 mm were used for the galvanizing experiments. The steel panels were thoroughly cleaned in three stages; (i) ultrasonic acetone cleaning for 10 minutes, (ii) alkaline cleaning in NaOH solution at 70°C for 10 minutes followed by scrubbing and rinsing in water, (iii) acid cleaning in dilute HCl at 50°C for 1 minute, scrubbing and rinsing in water. Finally the samples were treated with a Cu-based flux [12-14], whose composition was 4-6 % HCl, 3-5% SnCl₂, 0.1-0.25% CuCl₂.2H₂O. After fluxing, the panels were rinsed in water and dried prior to galvanizing under normal atmospheric condition.

The experimental galvanizing facilities included an electrically heated crucible furnace, SiC crucibles with a capacity of 3 kg of molten bath, a sample insertion machine and thermocouples. A eutectoid bath (Zn-22.3 wt % Al) was prepared for galvanizing (bath A). It was alloyed with: (i) 0.1 wt % Bi (bath B), (ii) 0.3 wt% of RE in the form of a master-alloy provided by Triebacher, Austria (bath C), and (iii) 0.2-0.4 wt% of Si in the form of Al-Zn-Si master alloy (bath D) (Table 1). The galvanizing temperature was varied between 530 and 600°C, and dipping time from 60 to 180 s. Experiments with bath A, B and C were repeated in a Rhesca galvanizing simulator under controlled reducing atmosphere to keep the metal surface free from oxides and render it very reactive. Instead of fluxing, the surfaces of the panels were cleaned and deoxidized by pretreating it at a temperature of 730°C for 30 s under a reducing (N₂ + 20% H₂) atmosphere, prior to galvanizing. The coatings developed here matched in quality with those obtained under

normal atmospheric laboratory conditions, hence the results obtained from bath A, B and C at the Rhesca simulator are reported here along with the results from bath D of the normal atmospheric laboratory conditions.

Coated samples were cut by a diamond blade, mounted and polished to study the through-thickness microstructure of the coatings in Hitachi S-3200M and Philips XL30-ESEM-FEG scanning electron microscopes (SEM). Energy dispersive spectroscopic (EDS) analysis, elemental mapping and elemental line scanning was conducted in Hitachi S-3200M and Hitachi S-4000 across the coating thickness. The process parameters of the representative samples investigated by SEM are given in Table 2.

The phases in the coating structure obtained with the bath D were analyzed with the help of X-ray diffraction (XRD) patterns obtained at the Philips Analytical X-Ray B.V. The sample was exposed in the as-coated condition, and also after polishing-off part of the coatings to study the phases present at different depths of the coatings.

Coating thickness measurements were carried out using an Elcometer 300, Model A300FNP23, 0-1250 μm range, on 20 locations on both faces of each coated sample. Their average is reported.

Field corrosion tests were conducted for 3 months at the Kure Beach, NC test site on the samples generated from all the above baths. Samples from two commercially produced grades of Zn-galvanized steels were also exposed for the purpose of comparison; one belonging to the more common galvanizing at 430°C (herein called theta-galvanized) and the other galvanized at 500°C (herein called delta-galvanized). Corrosion loss on field exposure was determined by washing away the products of corrosion from the surface of the coated products as per the ASTM G1 procedure; the samples were dipped in a 10 wt % ammonium persulfate solution for 30 minutes at room temperature, rinsed in running water and dried in air. This cleaning cycle was repeated six times. Three samples generated from each bath representing different dipping times were evaluated for corrosion loss and their average is reported.

Electrochemical corrosion test were carried out by determining the polarization resistance (R_p) on a Gamry Instruments' CMS 100 Corrosion Measurement System. A 3.5 wt% NaCl electrolyte was prepared with pH values of 3, 6.5 and 11 for this DC

corrosion test. The R_p data generated on 12 samples from each galvanizing bath was averaged and presented here as a comparative corrosion resistance behavior.

3.0 Experimental Results

3.1 Coating thickness

The coating thickness was measured as a function of bath temperature and dipping time. Fig. 1 summarizes the plots of the thickness of the coatings with time obtained from the experimental baths. A linear growth rate of the coating was observed in the case of bath A and bath B. The slope of growth rates at various temperatures are shown in Table 3. An increase in the slope with temperature is indicative of the increase of growth rate with temperature. The growth in the case of bath C showed a sharp change from a lower growth rate in the initial stages to a higher growth rate in the later stages, indicating a change in the mechanism of growth with passage of time. This also indicates that the initial beneficial effects of RE, reducing the coating thickness, is worn off in the later stages. The coatings obtained from bath D showed a parabolic growth suggesting a stronger influence of Si on coating behavior as compared with the Bi or RE addition.

3.2 Microstructures of the coatings

Typical through thickness microstructures of the coatings obtained from different bath compositions are shown in Fig. 2. The coatings exhibit three distinct layers which have been designated as interface layer (marked as A), intermediate layer (marked as B), and overlay (marked as C). The interfacial layer of the coating was generally found to be very adherent. As can be noticed from these micrographs the coatings obtained from bath A and B were very thick ($\sim 300\text{--}800\text{ }\mu\text{m}$), and also contained porosities large in number and size (Fig. 2a and b), whereas bath C showed a reduction in porosity (Fig. 2c) as well as in coating thickness ($\sim 200\text{--}700\text{ }\mu\text{m}$). The overall coating thickness obtained from the baths A, B and C were an order greater than the prevalent industrial norm of about $80\text{ }\mu\text{m}$. Besides higher thickness, the coatings produced by these baths were rough, dull in appearance and contained a high degree of discontinuities. In contrast, the coatings obtained from bath D were thin ($\sim 30\text{ }\mu\text{m}$), smooth and devoid of any porosity (Fig. 2d).

A closer examination of the substrate/coating interface of the samples from the baths A, B and C (Fig. 3a,b,c) shows random penetration of the reaction product into the substrate, which is indicative of the occurrence of bursting, whereas no such penetration was observed in the case of sample from the bath D (Fig. 3d). The occurrence and the effect of bursting is highlighted in Fig. 3b. Chemical analysis of this region (Table 4) indicates that the penetrating phase is an Fe-Al-Zn ternary phase having more Zn than elsewhere, and a Zn-rich unreacted pool of melt on the outer boundary of these bursts containing particles of the ternary Fe-Al-Zn phase. This phenomenon, though present in all the samples from baths A, B, and C, is especially pronounced in the case of bath B. A large compositional difference in these layers was noticed.

The thickness of the interfacial layer did not show an appreciable change on increasing the dipping time (from 70 to 90 s), at a given temperature (550°C) for bath C (Table 5), suggesting that, though the total coating thickness increased appreciably, the dense interfacial layer does not grow beyond a certain thickness. The interface, which appeared as a dark-grey, dense and homogenous layer next to the substrate was found rich in Fe and Al and lean in Zn in all cases. Table 4 summarizes the chemical composition of different regions. Fig. 4a shows elemental distribution in the intermediate layer across the columnar growth in the sample from bath C. The dark columns are found rich in Fe and Al, and the bright areas are Zn-rich. The elemental distribution in the intermediate layer of the sample from bath D is shown in the Fig. 4b. Fe and Al appear together everywhere with minor presence of Si, whereas Zn makes a contrast. Such morphology suggests a preference for the Fe-Al reaction over the Fe-Zn reaction.

The distribution of elements across the interface can best be illustrated by representing the elemental concentrations in the form of a line scan. The sample from bath C (Fig. 5) shows a homogeneous mix of an Fe-Al phase rich in Al, and a Zn-rich phase. It can be noticed from this scan that (i) the peaks of Al and Fe coincide whereas the peaks of Zn are in contrast with these elements, (ii) and there is no evidence of depletion of the elements across the interfacial layer. Spot analysis showed that the composition of the Fe-Al phase was close to Fe_2Al_5 (with Zn substituting for Al). The line-scan for bath D sample (Fig. 6), however, exhibits depletion of Si and Fe across the interfacial layer. The quantitative analysis of the interface layer has shown the presence

of substantial concentration of bismuth and silicon in bath B and D respectively, whereas bath C did not show any presence of RE in this layer (Table 4), or even in the intermediate layer.

The presence of high porosity in the intermediate layer has been noticed in the case of the coatings produced by baths A and B, whereas a relatively less porous intermediate layer has been observed in the coatings obtained with the bath C. Chemical analysis of several porosities indicated that many of them contained aluminum oxide particles in the center surrounded by a zinc-rich phase (Fig. 7).

The coating produced by bath D, on the other hand, did not show any porosity. The intermediate layer in bath D sample, on coarser level, showed the presence of a two-phase microstructure, where a few bright melt-like regions appeared in a predominantly gray phase (Fig. 8a). The gray phase (marked as B₁ in Fig. 8a) showed a composition close to Al-rich phase, whereas the bright phase, appearing like a flowing melt morphology (marked as B₂ in Fig. 8a), was found to have composition close to the Zn-Al eutectic point with negligible presence of Fe and Si (Table 4, 02). Upon magnifying the gray regions (marked as B₁) a well developed lamellar structure was revealed (Fig. 8b, c, d). Such morphology suggested the formation of the eutectoid microstructure in this region.

Some of the columns can be seen to grow upto the top layer of the coatings in the samples from bath A, B and C (Fig. 9), and the inter-columnar gaps appear filled with the Zn-rich phase. The bath D sample showed an overlay having an overall Zn-Al eutectoid composition (Table 4).

3.3 X ray analysis of phases encountered in the coating

Through thickness XRD patterns obtained from various regions of coatings, from the surface down to the interface, exhibited presence of various phases. The top surface of coating obtained from bath D showed the presence of Zn and Al only (Fig. 10a). In the intermediate layer (at a coating thickness of ~10 μ m) presence of the Fe₂Als phase along with the Al and Zn phases was noticed (Fig. 10b). Near the interfacial layer (at a coating thickness of ~5 μ m), the presence of relatively stronger peaks of the Fe₂Als phase indicated increasing volume fraction of this phase in regions close to interface layer (Fig.

10c). Finally, in the interface layer (at a coating thickness of ~ 2 μm) predominant presence of the FeaAls phase was noticed (Fig. 10d). Presence of Fe-peaks in this XRD pattern may be the result of exposure of the substrate at some places.

3.4 Corrosion Studies

Corrosion loss on field exposure at Kure Beach was found, on an average, to be 4.8, 3.1, 1.9 and 1.0 mils per year (mpy) for galvanized steel samples generated from baths A, B, C and D, respectively (Table 6), whereas it was 7.7 and 5.5 mpy for the commercially produced theta and delta galvanized steel samples, respectively. The galvanized samples from all the Zn-Al eutectoid baths, therefore, exhibited superior corrosion resistance compared with the conventional Zn-bath galvanizing, and among the various Zn-Al eutectoid baths studied, that containing Si yielded the best results.

The polarization resistance (R_p), which is inversely proportional to the current density (i_{corr}), provides a quick measure of the corrosion properties. The greater the value of R_p the higher would be the resistance against corrosion [15]. The polarization resistance curves (Fig. 11) indicate that addition of Bi and RE did improve the R_p values, and hence the corrosion resistance, of the coatings developed from the Zn-Al eutectoid bath to some extent but it was not a substantial improvement over that of the commercial zinc-galvanized steel. On the other hand, the coatings from the Si-treated bath showed about fifteen times greater resistance to corrosion as compared with the commercially produced Zn-galvanized steel at normal atmospheric conditions of pH=6, as well as at higher pH of 11. In acidic condition of pH=3, all the samples showed a lower resistance to corrosion.

4.0 Discussion

The results obtained in the present study of galvanizing in a Zn-Al based bath point towards the following important features:

1. The coatings formed have three distinct layers; interface layer, intermediate layer and overlay. The coatings produced by the binary Zn-Al, Zn-Al-Bi and Zn-Al-RE were porous and showed linear growth, whereas the coatings produced by Zn-Al-Si bath were non-porous and exhibited parabolic growth. A bursting phenomenon was

observed in the first three baths whereas Zn-Al-Si bath did not show any evidence of bursting.

2. Chemical analysis of different layers of coatings revealed that the interface layer was mainly composed of the Fe_2Al_5 phase, whereas the intermediate layer has shown the presence of two phases - one rich in Al and the other rich in Zn. A depletion layer was observed only in the case of coatings produced by Zn-Al-Si bath. Most of the porosities were found to contain Al oxide.
3. The eutectoid microstructure was observed in the case of coatings produced by Zn-Al-Si bath.

The coatings produced by the experimental baths exhibited different growth rates and morphologies. The growth kinetics, however, remained linear in all the cases except for the bath D which showed a parabolic growth. The line scan carried out across the interfacial layer did not show any depletion length for any element in the case of bath A, B and C (Fig. 5), indicating that the growth of the coatings was mainly interface controlled. In the case of the coatings produced by bath D, the presence of a depletion layer in the interface was observed indicating a diffusion-controlled growth process (Fig. 6). It is, therefore, pertinent to examine the interfaces in each of the coatings

4.1 Interface layer

The chemical and XRD analysis of coatings in all cases has shown that the interface layer (next to the substrate), which was dense and coherent, comprised mainly of ternary or quaternary derivative of the binary Fe_2Al_5 intermetallic phase. The binary Fe-Al [16] and Zn-Al [17] phase diagrams and isothermal sections of the Fe-Al-Zn [18] and Fe-Al-Si [19] ternary phase diagrams are shown in Fig. 12. It can be noticed from these figures that (i) the Fe_2Al_5 intermetallic phase has the highest liquidus temperature and therefore would be the first phase to solidify and, (ii) it has low solubility for other elements. Based on this information it can be inferred that during the initial stages, the phase reaction is dominated by the formation of the Fe_2Al_5 intermetallic phase. This observation is in agreement with that reported by Perrot et al. [20] who have shown that during the initial stage, the formation of FeZnAl_5 occurs, which is subsequently replaced

by the Fe₂Al₅ phase. It has also been shown that if the Al content in the bath exceeds beyond 0.15 wt%, the Fe₂Al₅ becomes the thermally stable phase [21] and under these conditions an extended solubility of Zn up to 22 wt% in the Fe₂Al₅ phase occurs [22]. Since, in the present study, the formation of the FeZnAl₅ phase has not been observed in the interface layer and no microstructural evidence has been obtained anywhere for prior presence of the FeZnAl₅ phase in the interface, we conclude that the Fe₂Al₅ phase has directly formed from the liquid phase.

Guttmann [23] has estimated the average Zn diffusion coefficient in the FeAl₅ phase as 5×10^{-11} cm²/s at around 460°C. Based on this value, a rough estimate of the diffusion length $\{x \sim (Dt)^{1/2}\}$ of Zn in the FeAl₅ phase should be in the range of 0.55 μ m (60 s) to 0.95 μ m (180 s). This is two order less than the estimated thickness of the interface in the present study. Based on this estimate we infer that the lower concentration of Zn could be due to the fact that high concentration of Al is present in the present experiments, which (i) reduced the relative concentration of Zn and/or (ii) caused a more vigorous exothermic reaction between Fe and Al [24] resulting in higher temperatures at the interface and hence faster diffusion of Zn from the FeAl₅ phase, either towards the substrate or back to the bath. It is worth mentioning here that evidence of bursting have been noticed in the case of samples coated by bath A, B and C (Fig. 2) and the chemical composition of the burst region has shown the presence of a high Zn concentration (Table 4). This suggests that diffusion of Zn has occurred from the Fe₂Al₅ phase during the coating process.

Tang [25] has shown that in dilute Al (<1 wt%) baths the formation of the FeAl₅ phase is a two-step process. The first stage is associated with the uptake of Al, which is controlled by the continuous nucleation of the Fe₂Al₅ phase, and second stage is a diffusion controlled growth process of the Fe₂Al₅ phase. In the present case, since the concentration of Al was high (~23 wt%) the availability of Al in the vicinity of the growing front would not be the controlling step. In fact, the line scan of concentration of Al did not show any depletion. In contrast the lower concentration of Zn in the Fe₂Al₅ phase (Table 4) and the presence of a two-phase microstructure in the top portion of the interface layer suggest that probably the rejection of Zn from the Fe₂Al₅ phase was the rate-controlling step. The column of Zn-rich phases in the interface layers can be noticed

in Fig. 3b. Interestingly, the average separation between these columns is approximately 1-2 μm , which is twice the diffusion length estimated and hence could be taken as indirect evidence in support of the above argument. Furthermore, the thickness of the interface layer determined for varying dipping time for bath C sample was found to be of the same order ranging between 60 to 180 μm with average of about 100 μm , whereas in the case of coatings produced by bath D the thickness of the interface layer was only about 4 μm . The negligible growth of the interfacial layer thickness during the dipping time of 60 to 120 s, as opposed to a three to six times growth of the intermediate layer, indicates that the growth of the dense interface layer stops at a certain level, after a rapid growth in the initial stages of the dipping.

4.2 Intermediate layer

The intermediate layers observed in all the coatings have multiphase microstructures (for example, Fig. 3). Strong solute partitioning between Fe, Al and Zn causes the formation of a Zn-rich phase and an Al (Fe)-rich phase. The morphology of this layer with the interface layer underneath suggests that the formation of the Fe-Al phase has occurred first during the solidification process rejecting the excess of Zn. It appears that the formation of the intermediate layer starts when the concentration of Zn builds up ahead of the moving interface causing instability at the interface. In some of the regions the formation and growth of the Fe-Al phase continues the rejection of Zn into the inter-columnar space, causing the latter to become rich in Zn. The Zn-rich regions, having a lower liquidus temperature [17], remained liquid at lower temperatures, thus solidifying the last. The composition of some of such Zn-rich areas has been found to approach the Zn-Al eutectic composition (Fig. 12b). The growth of the intermediate layer shows the presence of Fe bearing Al-rich phase.

Selverian et al. [24] have reported that without Si in the bath the reaction zone flakes off, whereas with Si the reaction zone is adherent. This solid reaction layer at the interface acts as a diffusion barrier for the reactive species, thereby reducing the reaction rate between the iron panel and the bath by several orders of magnitude as compared with the binary Al-Zn baths. In the case of bath D, paucity of Fe at the moving front would be the rate-controlling step as evident from the line scan shown in Fig. 6. Lower

concentration of Fe at the moving front would retard the rate of formation of the Fe_2Al_5 phase, as Al shows high solubility of Fe under metastable conditions. The XRD pattern from this region (Fig. 1Ob) failed to show a high volume percentage of the Fe_2Al_5 whereas the chemical composition of this region showed concentration of Fe in the Al rich phase far greater than predicted by the phase diagram.

The sluggish growth of the Fe_2Al_5 phase would allow other phases like Al rich phase to start solidifying. The morphological evidence in support of this argument is: (i) The formation of Al-rich and the Zn-rich regions at the coarser level in the

intermediate layer just ahead of the interface layer (Fig. 8a) indicates solute partitioning causing phase separation, (ii) The chemical composition of the Zn rich regions being close to the eutectic

composition suggests that the last phase to solidify had the lowest liquidus temperature.

The subsequent cooling of these phases has resulted into the formation of lamellar structure indicating the occurrence of the eutectoid phase reaction. However, further investigations are needed to establish the exact mechanism and the sequence of transformation.

The intermediate layers of the coatings produced by baths A, B and C show varying degree of porosity. Chemical analysis shows that many of these porosities contained Al-oxide particles in the center, surrounded by a Zn-rich phase. The presence of Al-oxide particles in the middle of the porosities clearly indicates that the porosities formed from these particles. The oxide layer formed at the top of the bath breaks-up when the steel panel is inserted into the bath, and small particles of these oxides may have floated around the substrate and become trapped in the Zn-rich phase, which remain liquid even when the sample is withdrawn from the bath. Subsequent solidification of such liquid phases would cause shrinkage resulting in development of high stresses between oxide particles and the matrix. The stresses would cause separation of these particles from the matrix because the poor wettability of the oxide particles with the liquid phase minimizes the opportunity for any chemical bonding between them. The growth rates of the entire coating obtained from the bath A, B and C have shown a similar reducing trend indicating an interrelation between the porosity and the growth

rate. The coating produced by bath D, containing Si, had a uniform two-phase microstructure in the intermediate layer. It did not show any porosity and at the same time it produced the lowest thickness. This also points toward the effectiveness of the alloying elements in controlling the growth as well as porosity of the coatings.

4.3 *Top coating layer*

The drag-out layer of liquid metals, when the steel panel is withdrawn from the bath, is thicker when the bath viscosity is higher. Thus, lowering of bath viscosity, for example with Si addition, would contribute towards reduction in the coating thickness. The drag-out layer, also called overlay, solidifies on cooling to form the top coating layer exhibiting the bath chemistry. The top coating layer from bath D showed exactly this phenomenon by exhibiting the Zn-Al eutectoid composition (Table 4). On the contrary, the reaction product was evident right upto the top of the coatings in the case of baths A, B and C, where some of the columnar growth of the Fe-Al-Zn ternary phase could be seen to continue from the intermediate phase upto the top of the coatings. The inter-columnar spaces were found filled with the Zn-rich phase. This indicates that the reaction between Fe and the drag-out molten bath continued even after the panel was withdrawn from the bath, probably facilitated by the heat generation due to the exothermic reaction between Fe and Al [24]. As the bath D showed no evidence of the reaction product in the top layer, it can be inferred that addition of Si into the bath could successfully suppress the exothermic reaction.

4.4 *Corrosion behavior of the coatings*

It was observed that there was an increasing order of corrosion resistance (Table 6) and decreasing order of porosity in the coatings from bath A, B and C, respectively (Fig. 2). The coating from bath D was completely free from porosity and showed the greatest resistance to corrosion. There appears a correlation between the degree of porosity and corrosion property of the coating, which agrees well with the explanation provided by Goodwin [26] that a porous zinc oxide superficial layer forms on the surface by a mechanism of dissolution/reprecipitation, leading to preferential corrosion pathways across the high porosity areas. This explains why the corrosion resistance was minimum

in case of the coating that had highest porosity (bath A), and highest in case of the most dense coating (bath D). Apart from the structural density, the Fe-Al-Zn alloy phase has superior corrosion resistance [27, 28]. The intermediate and the top coating layers from baths A, B and C exhibit predominantly Fe-Al-Zn intermetallics (darker phase) interspersed with a Zn-rich phase (brighter phase) where the Zn-corrosion products get trapped and acts as further barrier to corrosion [29]. The coating surface obtained from baths A, B and C were very rough, varying between Ra 13 and 78, with the higher numbers belonging to baths A and B, and the lower numbers to bath C [30]. Since the electrochemical corrosion test determines the corrosion behavior of the surface, the surface condition, such as roughness, influences these observations. In the polarization resistance test, a coated surface area equivalent to 2.54 cm diameter was exposed for all the samples. However, the peaks and valleys on a rough surface increases the effective surface area of the coating exposed during the test, and therefore the corrosion rate obtained on a rough surface would be erratic and on the higher side when compared with that obtained on a smooth surface. This appears to be the reason for the lower values of polarization resistance (R_p) obtained for samples from bath A, B and C (Fig. 11). The samples from bath D exhibit a smooth and dense coating, and the R_p values for these samples were several times greater than all other samples. Thus, both the field exposure, as well as the electrochemical tests indicate that greater corrosion resistance values were obtained from the Zn-Al eutectoid bath primarily because of: (i) the alloy phases developed in the coating, (ii) a smooth coating surface, and (iii) a dense coating layer.

4.5 Role of ternary additions

Ternary additions were carried out into the bath with the aim of reducing the rate of growth of the coatings and arresting porosities. In the present study, it has been observed that the quality of the coatings depends primarily upon the following factors:

- The ease with which Fe and the reactive species from the bath can diffuse towards each other through the interface layer.
- concentration of the oxides of Al in the bath which appears to control the porosity.
- viscosity of the liquid phase which reduces the overlay layer.

A relatively higher concentration of Bi in the interface layer with bath B indicates

that Bi has a moderate solubility in the Fe-Al intermetallics and a marginal reduction in the growth rate could be attributed to this fact. However, Bi was not very effective in controlling the diffusion of Fe, as the rate of growth remained linear throughout the coating process, indicating dominance of interface control growth. The main contribution of Bi is in reduction of viscosity of the liquid phase. It has been shown that addition of 0.1 wt% Bi in the Zn bath reduces the surface tension from 550 to 475 mJ/m² [31]. Lower viscosity reduces the chances of entrapment of Al-oxide into the liquid phase, hence resulting in a lower porosity in the intermediate layer.

The role of the rare-earth elements appears to be more complicated, as these elements have not been found in either the intermediate or interfacial layer. However, the presence of these elements has been noticed at the top of the overlay layer (Fig. 13). The growth rates of the coatings have shown two types of behavior: a retarded growth rate in the initial stages and an accelerated growth in the later stages indicating presence of a break-off point (Fig. 1c). This effect has been observed at all the temperatures, and the higher the temperature, the sharper is the change in growth rate. In order to understand the role of the RE elements, spot analysis and the line-scan on a sample which was dipped for a very short time (40 s) in bath C, was carried out (Fig. 14). The presence of RE elements, especially in the zinc-rich regions, in the interface layer could be observed. Based on these observations, it can be inferred that RE elements, due to limited solubility in the Fe-Al phase, were rejected into the bath or Zn-rich regions and hence the effects were worn-off in the later stages of coatings. This confirms the findings of Yang [32] who reported that the RE elements segregate at the coating/substrate interface, postponing the formation of a detectable interfacial inhibition layer, suggesting a major role of these elements in stabilizing the interfacial layer. However, detailed investigations are needed to corroborate these findings.

Si has been found to be the most effective ternary addition in the Zn-Al bath in terms of reduced coating thickness, uniformity of microstructure and corrosion resistance. The presence of a high concentration of Si in the interface layer clearly indicated that along with Al, Si has also participated in the reaction. The beneficial role of Si can be attributed to the fact that: • it lowers the solidus temperature of the intermetallic compound and hence formation

of the phase occurs at lower temperatures [18]. This reduces the structural inhomogeneity due to smaller differential in solidification temperatures of the different phases.

- it reduces the diffusivity of solid Fe and the reactive species of the molten bath towards each other and hence retards the growth rate of coatings. Similar findings were reported by Neemuchwala et al. [33], who inferred that Si removes Fe from the reacting system, delaying Fe-Zn phase formation, such that a continuous inhibiting Fe-Al phase layer had a chance to form.
- It increases the bath fluidity [11] and reduces the Al-oxide in the bath [34] which drastically minimizes the occurrence and entrapment of the Al-oxide particles in the bath, therefore yielding a coating free from porosities.

These factors together reduce the thickness of the interface layer and also control the overall thickness of the coatings, which are free from porosities. The thin, smooth and dense coatings exhibit excellent corrosion resistance. The thin coatings of about 20-30 μm is especially suitable for preformed threaded parts such as nuts and bolts. This Si treated Zn-Al eutectoid galvanizing alloy appears to be a good candidate to address the environmental concern regarding leaching of zinc.

5.0 Conclusions

The major findings of galvanizing in a Zn-Al eutectoid bath can be summarized as follows:

- The coatings from the Zn-Al eutectoid galvanizing bath show a dense interfacial layer, a mixed phase intermediate layer and an overlay. The interfacial layer shows evidence of bursting at the metal/coating interface, and the intermediate layer exhibits a large number of porosities. The addition of Bi and RE as minor alloying elements did not appreciably change the coating morphology.
- The coating thickness growth in a Zn-Al eutectoid bath remained linear even on addition of Bi as well as RE. However, the rate of growth tapered a little with Bi addition, and reduced to a greater extent on the addition of RE. The degree of the linear growth rate appeared to be associated with the roughness of the coating surface,

the porosities in the intermediate coating layer, and occurrence of bursting at the interface.

The porosities nucleated around the trapped Al-oxide particles in the Zn-rich melt in the coating matrix, and appeared proportional to the degree of the growth rate and occurrence of bursting at the metal/coating interface.

Addition of 0.2-0.4 wt% Si in the bath changed the interface-controlled linear growth to diffusion-controlled parabolic growth. A coating as thin as 10-40 μm could be achieved. The bursting at the interface, and the porosities in the intermediate layer were totally eliminated. The surface of the coated product appeared bright and smooth.

The corrosion resistance of the coatings from the Zn-Al eutectoid galvanizing alloy was greater than that from the zinc galvanized coatings, and the minimum corrosion losses were observed in the case of smooth and dense coatings obtained from the Si treated bath.

The Si-containing bath shows great promise for future galvanizing of steel.

Acknowledgements

The authors are extremely thankful to the Weert Groep, The Netherlands, who continue to sponsor this research and development work at the University of Cincinnati. The help rendered by the Advanced Characterization Center, University of Cincinnati, is gratefully acknowledged. We are thankful to the Eastern Alloys, Inc (NY), Triebacher (Austria), the Witt Galvanizers (Cincinnati), the Noranda Corporation (Canada) for free supply of metals and alloys needed for the experiments, and to the Zinc Corporation of America (ZCA) for carrying out the bath analysis for us. Our thanks are due to Tatu Muukkonen of VTT Manufacturing Technology (Finland) for facilitating the experiments in the Rhesca Galvanizing Simulator.

References

1. Jordan C.E, and Marder A.R: *J Mater.Sci.*, 1997, vol.32, p.5593
2. Tang N-Y, and Adams G.R: *The Minerals Metals and Mater. Society*, 1993, p.41-54
3. Perrot P, Tissier J-C, and Dauphin J-Y: *Z.Metallkd*, 1992; 83:11
4. Lin K.L, Ho J.K, Jong C.S, and Lee J.T: *The Minerals, Metals and Mater. Society*; 1983, p.89-97
5. Hisamatsu Y: Galvatech'89, Tokyo, *ISIJ*, 1989, p.3
6. Goodwin FE: In: Krauss G, Matlock DK, editors. Zinc based steel coating systems: Metallurgy and Performance. Warrendale, PA: TMS, 1990, p.183
7. Aoki T, Miyoshi Y, and Kittaka T: Galvatech'95, Chicago, IL: *Iron and Steel Society*, 1995, p.463
8. Marder AR: Materials selection and design, ASM Handbook, 1997, vol.20, p.470
9. Townsend HE, and Borzillo AR: Galvatech'95, Chicago, IL: *Iron and Steel Society* , 1995, p. 171
10. Marder A.R: *Progress in Mater. Sci.*, 2000, vol.45, p. 191-271
11. Mondolfo L.F; Aluminum alloys: Structure and properties; Butterworth, Boston, 1976, p.843-844
12. Van Ooij W.J, and Prasanna V: US Patent 6,372,296.
13. Van Ooij W.J, and Prasanna V: US Patent 6,200,636.
14. Van Ooij W.J, and Ranjan M: *5th Asian Pacific General Galvanizing Conference*, Busan, Korea, October 21-25, 2001, p.73-88
15. Jones D.A: Principles and prevention of corrosion; Prentice Hall, NJ, 1996, p. 146-152
16. Thaddeus B Massalski: Ed-in-Chief, Binary alloys phase diagram, Vol.1, p.112
17. Thaddeus B Massalski, Ed-in-Chief, Binary alloys phase diagram, Vol.1, p.185
18. Villars P, Prince A, and Okamoto H: Handbook of ternary alloy phase diagram, ASM International, 1997, vol.3, p.3664
19. Villars P, Prince A, and Okamoto H: Handbook of ternary alloy phase diagram, ASM International, 1997, vol.3, p.3606
20. Perrot P, Tissier J-C, and Dauphin J-Y: *ZMetallkd*, 1992, vol.83, p.11

21. Lepretre Y, Mataigne J.M, Guttman M, and Philibert J: In: Goodwin F.E, Editor; Zinc based steel coating system: Production and performances; Warrendale, PA, IMS 1998, p.95
22. Chen ZW, Sharp R.M, and Gregory J.T: *Mater. Sci. Technol.*, 1990, vol.6, p.1173
23. Guttman M, Lepretre Y, Aubry A, Roche M-J, Moreau T, Drillet P, Mataigne J.M, and Baudin H: Galvatech'95, Chicago, IL, *Iron and Steel Society*, 1995, p.295
24. Selverian J.H, Marder A.R, and Notis M.R: *Met. Trans.*, 1989, vol.20A, p.543
25. Tang N-Y: *Met. Trans.*, 1995, vol.26A, p. 1669
26. Goodwin F.E: In Krauss G, Matlock D.K, editors. Zinc based steel coating systems-Metallurgy and performance. Warrendale, PA. TMS, 1990, p. 183
27. Tatsumi I, Yoshihiko T, Tetsuya N, Koshi T, and Masamichi Y: *Proc. of 1st Asian-Pacific Galvanizing Conf.*, Sep 15-18, 1992, p.158-166
28. Kubota H, Kazuhiko T, Yasuhiro T, and Junichi T: *Proc. of 1st Asian-Pacific Galvanizing Conf.*, Sep 15-18, 1992, p.149-157
29. Zocolla J.C, Townsend H.E, Borzillo A.R, and Morton J.B; In: Coburn S.K, Editor; Atmospheric factors affecting the corrosion of engineering metals; ASTM STP 646, Philadelphia, PA: ASTM 1978, p. 165
30. Ranjan M: Development of a new Zn-Al eutectoid alloy for hot-dip batch galvanizing, MS Thesis, University of Cincinnati, March 17, 2003, p.29
31. Gagne M: *Metall.* vol.53, Jahrgang. Nr.5/99, p.269-271
32. Yang Y, and Yu Z: *Acta Met. Sin.*, 1993, vol.29A, p.540
33. Neemuchwala N.D, and Hershman A.A: *Proc. 7th Int'l Conf. Hot Dip Galvanizing*, Paris, 1964, Zinc Development Association, Pergamon Press, Oxford, 1967, p. 179
34. Sebisty J.J, and Palmer R.H: *Proc. 7th Int. Conf., Hot Dip galvanizing*, Paris, 1974, Zinc Development Association, Pergamon Press, Oxford 1967, p.235

Figure captions

Fig. 1 Graphs showing coating thickness as function time and temperature obtained from (a) Zn-22.3 wt% Al bath (b) Zn-22.3 wt% Al-0.1 wt% Bi bath (c) Zn-22.3 wt% Al-0.3 wt% RE bath and (d) Zn-22.3 wt% Al-0.3 wt% Si bath. Linear growth is noticed in case of (a) and (b), whereas (c) shows two types of linear behaviour and, (d) shows parabolic growth. The slope and other relevant parameters for each curve are listed in Table 3.

Fig. 2 Showing typical cross sectional microstructures of the coatings obtained from the four baths. Three distinct layers in the coatings are marked as A (interface layer), B (intermediate layer) and C (overlay) in all the figures, (a) Thick coating and presence of large number of porosity in the coating obtained from the binary Zn-22.3 wt% Al bath could be noticed from the figure. Relatively lower number of porosities in the coatings produced by Zn-22.3 wt% Al-0.1 wt% Bi bath (b) and by Zn-22.3 wt% Al-0.3 wt% RE bath (c) is evident in the figures, (d) Very thin coating with nearly no porosity in coating from Zn-22.3 wt% Al-0.3 wt% Si bath could be noticed from the figure.

Fig. 3 SEM micrographs showing the interface layer obtained from the four baths; (a) Zn-22.3 wt% Al bath (b) Zn-22.3 wt% Al-0.1 wt% Bi bath (c) Zn-22.3 wt% Al-0.3 wt% RE bath and (d) Zn-22.3 wt% Al-0.3 wt% Si bath. The presence of bursting phenomenon and fragments of the inhibition layer could be clearly noticed in (a) and (b). Zn rich regions penetrating inside the substrate is also evident in these micrographs. A magnified view of the burst regions showed presence of cracks at the interface (c). Columns of Zn rich regions aligned in the growth direction could be clearly noticed in micrograph shown in (b). Presence of dense interface layer and no evidence of bursting can be observed in (d).

Fig. 4 Elemental map of the coatings produced by bath C and D. (a) Shows the distribution of Fe, Al and Zn in the coating from bath C. For the purpose of comparison, a secondary electron image is also shown. Clear separation of Zn-rich and Al(Fe)-rich phases could be noticed from this figure, (b) Shows the distribution of Al, Fe, Zn and Si in the coating from bath D. The presence of alternate regions of Zn-rich and Al(Fe)-rich

phases and lamellar structure suggests the formation of eutectoid microstructure. However, due to low Si content a poor contrast was observed in the Si elemental map.

Fig. 5 Line scan obtained across the interface layer of the coating produced by bath C (bath temperature: 550°C, dipping time 80 s). A sharp drop in the concentration of elements (Al and Fe) across the interface (marked in the figure) between the substrate and the interface layer indicates interface control growth of the coating as was observed in the case of Fig. 1. The reversal in the peaks between Al and Zn indicates strong solute partitioning. Higher concentration of Fe even in the regions away from the interface indicates no depletion of Fe at the moving front.

Fig. 6 Line scan obtained across the interface layer of the coating produced by bath D. Presence of a depletion layer across the interface (marked in the figure) between the substrate and the interface layer indicates diffusion-controlled growth of the coating in this case. This is in agreement with the growth rate shown in Fig. 1(d).

Fig. 7 Secondary electron image showing the presence of porosity in the intermediate layer. Many such porosities were found containing Al-oxide particles, as marked in the figure.

Fig. 8 Secondary electron images showing the presence of eutectoid microstructure in the coatings produced by bath D. (a) lower magnified view of the coating (x2000) showed presence of gray and white regions marked as B₁ and B₂ in the micrograph. Chemical analysis of these phases is listed in Table 4. (b)-(d) High magnified view of gray regions showed a very fine distribution of the lamellar structure.

Fig. 9 Micrographs showing the top layer (overlay) in samples from (a) bath A, (b) bath B, (c) bath C and, (d) bath D. Columnar growth of the Al rich phase right up to the top could be noticed in (a)-(c), whereas clear separation between the intermediate layer and overlay can be observed in (d).

Fig. 10 XRD patterns obtained through-thickness of the coatings produced from bath D. (a) XRD from the coating surface. Peaks in this XRD could be indexed in terms of the fee Al and hep Zn. Absence of any other phase indicates solidification of the bath without undergoing any phase reaction, (b) XRD from intermediate layer (-10 (im coating thickness). Faint peaks pertaining to the Fe_2Al_5 phase along with the Al and Zn phase can be observed, (c) XRD from intermediate layer (~5 p,m coating thickness) shows relatively stronger presence of the Fe_2Al_5 phase, (d) XRD from the interface layer (-2 u,m coating thickness) showing predominant presence of the Fe_2Al_5 phase along with Fe peaks which presumably were contributed from the substrate and traces of Zn.

Fig. 11 Corrosion resistance determined through measurement of polarization resistance (R_p) as a function of pH value of the electrolyte. The galvanized steel from Zn-Al-Si bath shows the greatest resistance to corrosion at the most commonly encountered environment having pH -6.5.

Fig. 12 (a) Binary Fe-Al phase diagram [16], (b) binary Zn-Al phase diagram [17], (c) isothermal section of ternary Fe-Al-Zn phase diagram at 575°C [18] and, (d) isothermal section of ternary Fe-Al-Si phase diagram at 600°C [19].

Fig. 13 EDS analysis of the top layer of the coating produced by bath C showing presence of rare-earth elements in this layer.

Fig. 14 Line scan obtained across the interface layer of the coating produced by bath C (temperature 530°C, dipping time: 40 s). The presence of Ce in the Zn rich phase can be concluded from this line scan.

Table 1 Chemical composition of the experimental baths used in this study

Bath	Additive	Al	Bi	La	Ce	Si
A	None	22.1	-	-	-	-
B	Bi	22.1	0.10	-	-	-
C	RE	22.7	-	0.13	0.19	-
D	Si	22.2	-	-	-	0.3

Table 2 Process parameters of the samples selected for microstructural investigation.

Sample #	Bath	Additive	Bath Temp(°C)	Dip Time(s)
1	A	None	530	80
2	B	Bi	540	80
3	C	RE	540	80
4	D	Si	590	120

Table 3 Coating thickness growth rate for the experimental baths

Temperature (°C)	Linear behavior, slope of the curve um/s				Nonlinear behavior 'Y = t ⁿ ;n'	
	Zn-Al	Zn-Al-Bi	Zn-Al-RE		Zn-Al-Si	
			Initial stage	Later stage	0.03 Si	0.035 Si
530	11.9	10.14	4.4	5.8	0.48 (555 °C)	0.58 (600 °C)
540	13.9	13.74	8.55	10.75		
550	14.07	16.66	9.2	17.4		

Table.4 Chemical analysis of coating layers as per EDS

Bath	Fe		Al		Zn		Bi		Re	Si		Remarks
	wt%	at%	wt%	at%	wt%	at%	wt%	at%	%	wt%	at%	
Interfacial layer												
A	46.5	40.0	19.7	35.1	33.8	24.9	-	-	-	-	-	Bursting
B	46.4	35.5	30.1	47.6	18.3	11.9	3.6	0.7	-	-	-	Bursting
C	57.6	45.8	23.4	38.4	17.7	12.0	-	-	-	-	-	Bursting
D	43.3	29.4	43.1	60.6	10.8	6.3	-	-	-	2.8	3.8	Fe ₂ Al ₅
Intermediate layer (Dark gray phase)												
A	23.8	21.0	19.8	36.3	56.5	42.7	-	-	-	-	-	
B	35.1	30.2	24.8	44.2	24.4	17.9	14.1	3.2	-	-	-	
C	30.5	22.3	31.5	47.7	34.7	21.7	-	-	-	-	-	
D	30.0	21.7	30.2	45.3	33.3	20.6	-	-	-	3.9	5.6	
Intermediate layer (Brighter phase)												
B	4.4	4.7	3.8	8.5	84.9	77.8	4.8	1.4	-	-	-	
C	2.9	3.0	2.9	6.3	92.0	82.5	-	-	-	-	-	
Di	0.9	0.8	19.2	36.4	79.6	62.3	-	-	-	0.3	0.5	Eutectoid
D ₂	0.8	0.9	4.7	10.7	94.3	88.0	-	-	-	0.2	0.4	Eutectic
Top Layer (Dark gray phase)												
A	30.9	25.3	26.3	44.6	42.9	30.1	-	-	-	-	-	
B	41.0	28.9	39.7	57.8	12.9	7.8	4.5	0.8	-	-	-	
C	27.1	21.3	27.2	44.3	43.8	29.4	-	-	-	-	-	
Top layer (Brighter phase)												
B	7.1	7.0	7.7	15.7	79.7	67.1	2.8	0.7	-	-	-	
C	5.9	5.9	8.4	17.4	84.4	72.2	-	-	-	-	-	
D	2.4	1.9	22.9	39.3	72.1	51.1	-	-	-	-	-	Eutectoid
Porosity: Particles and the surrounding bright phase												
Bath	Fe		Al		Zn		Oxygen		Re	Si		Remarks
	wt%	at%	wt%	at%	wt%	at%	wt%	at%	%	wt%	at%	
C	0.5	0.2	56.1	44.8	3.8	1.1	40.1	53.9	-	-	-	Particle
C	5.4	4.6	26.8	46.6	67.8	48.8	-	-	-	-	-	Vicinity

Table.5 Growth of coating layers with time in bath C at 550°C

Dipping Time, s	Total Thickness, um	Interfacial layer thickness, um			Growth Beyond Interface, jam
		Min	Max	Average	
70	379	67	135	95	284
80	470	68	139	100	370
90	727	63	154	114	613

Table.6 Corrosion losses on field exposure

Bath	Corrosion loss, mpy		
	Min	Max	Average
Zn-theta (Standard HDG)	7.24	8.11	7.67
Zn-delta (High temperature HDG)	4.82	6.12	5.47
A	3.45	5.09	4.82
B	1.87	4.25	3.08
C	1.65	2.02	1.85
D	0.64	1.28	0.96

We have now invented a Zn-Al alloy system that contains other metals in low concentrations. The new composition influences the quality of coating in several ways, viz;

- The Fe-Al reaction is controlled to yield coating thickness anywhere in the range of 20-100 μm , which is of great interest to many end uses like in the fastener industry. Threads of nuts and bolts cannot tolerate more than 20-30 μm for a protective coating.
- Eliminates the Fe-Zn outburst, thereby improves the surface roughness.
- The new composition yields corrosion resistance much higher than that of the conventionally hot dip batch galvanized steel. The corrosion resistance manifested itself in electrochemical linear polarization measurements in the laboratory, and also in field exposure tests at the Kure beach site of the Laque Center.

These spectacular improvements were obtained essentially by addition of silicon in the Zn-23 wt % Al bath and raising of the bath temperature from 530-550 to 580-600°C. The silicon addition retards the onset of the outburst formation, and also retards the reaction between Fe and Al, thus excellent control in coating thickness. The increase in corrosion resistance could be the result of formation of a compact and pore-free coating layer.

With the new addition our process is as follows:

- Bath composition: (Zn) + (23 wt % Al) + (0.2 - 0.4 wt % Si) *(0.01-0.08 wt % Si)* *Manjiv*
- Fluxing: Cu-Sn flux, according to the US Patent No.6,372,296, with fluxing time of 60 s.
- Bath temperature: 580-600°C
- Dipping time: 60-180 s.
- Cooling: in ambient

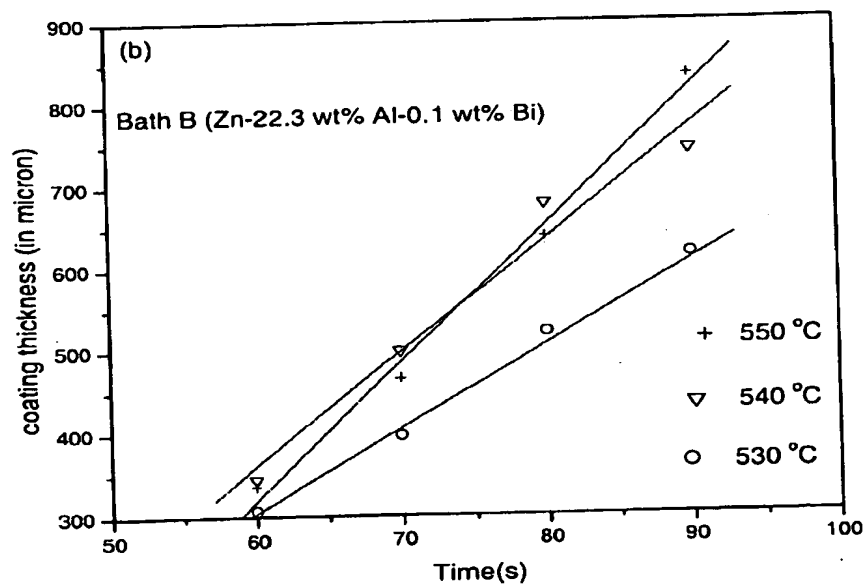
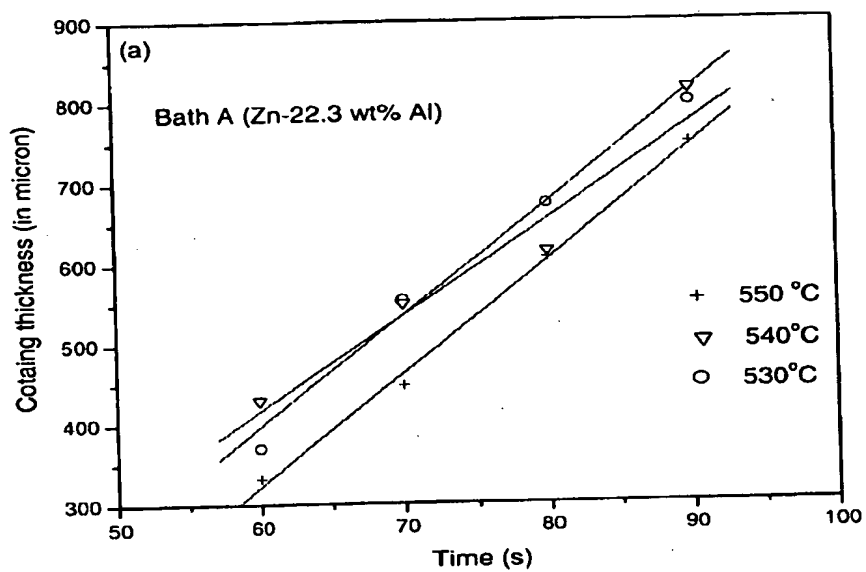


Fig. 1a,b

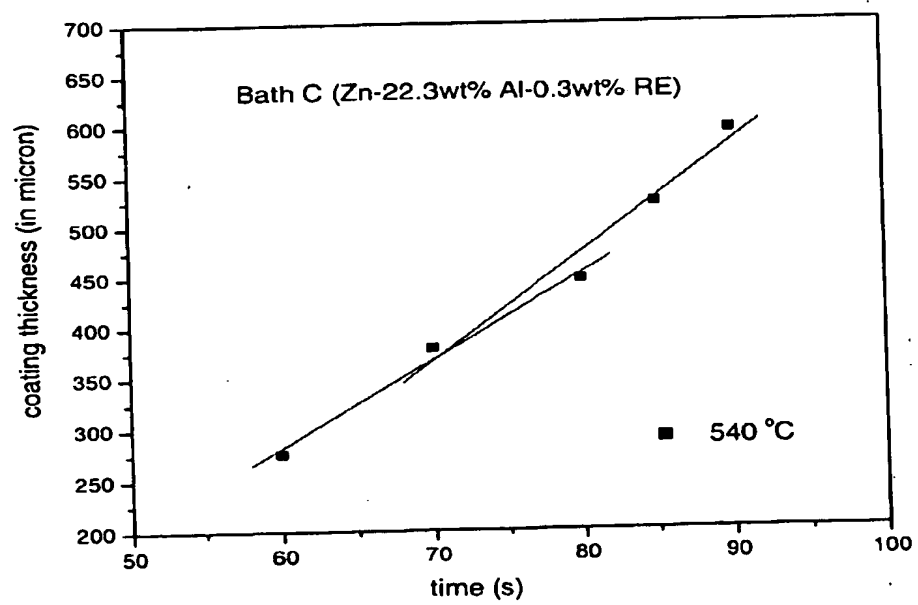
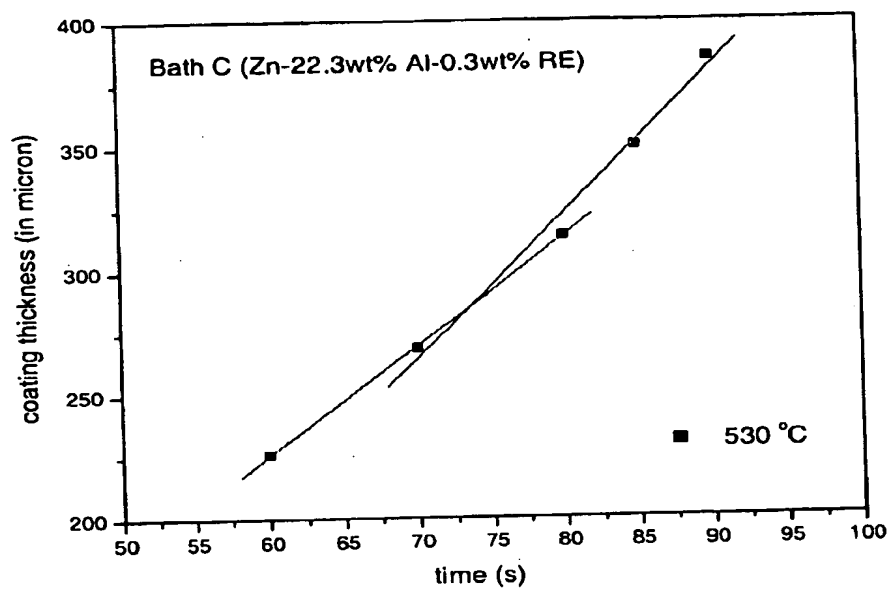


Fig. 1c

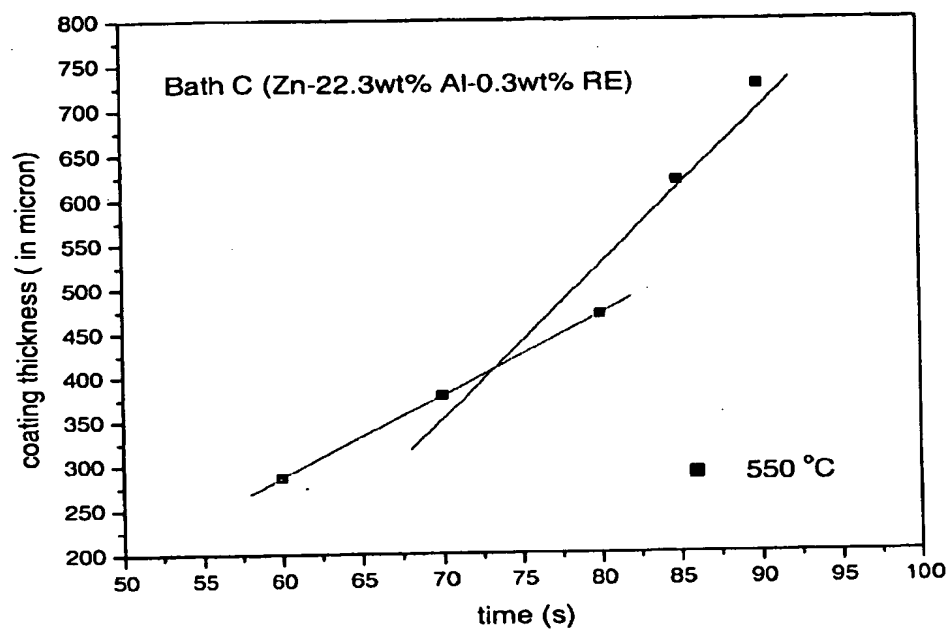


Fig. 1c

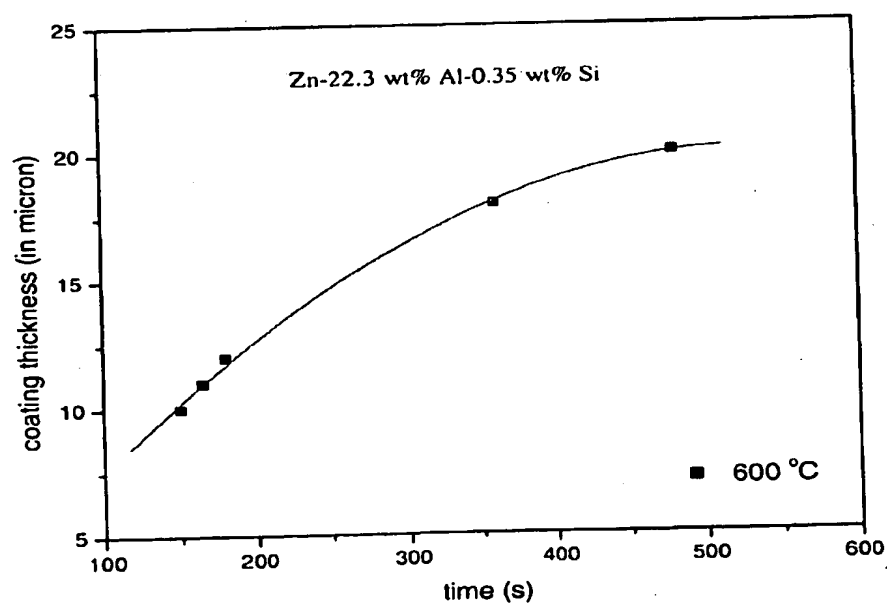
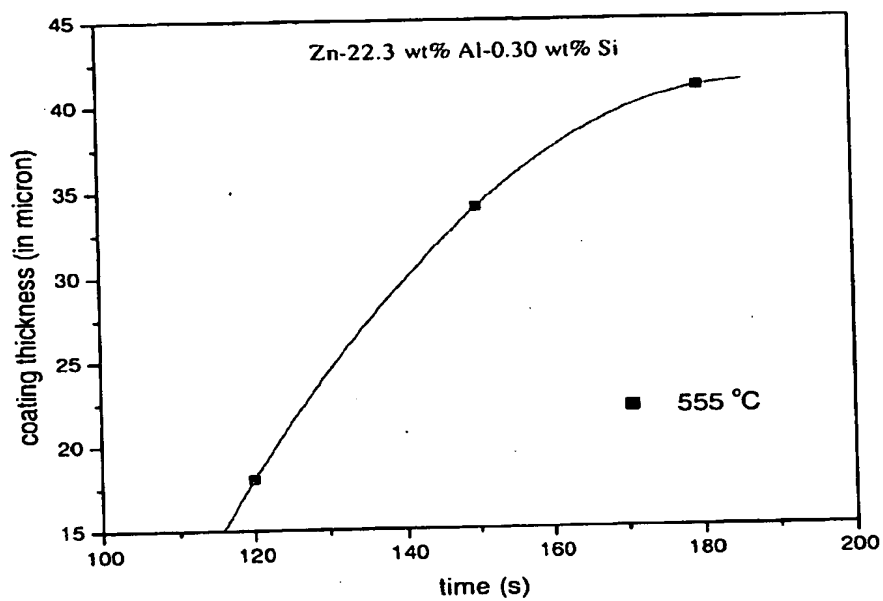


Fig. 1d

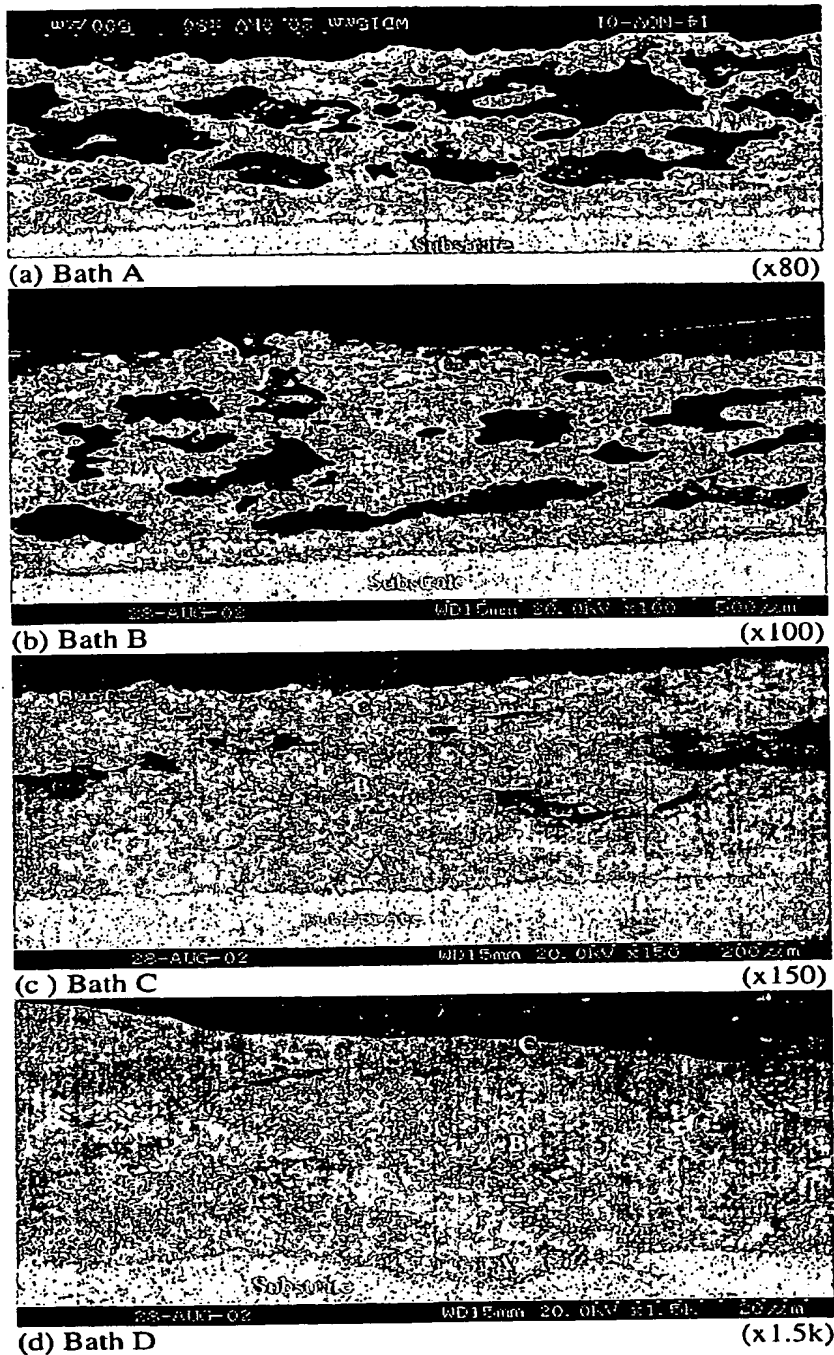
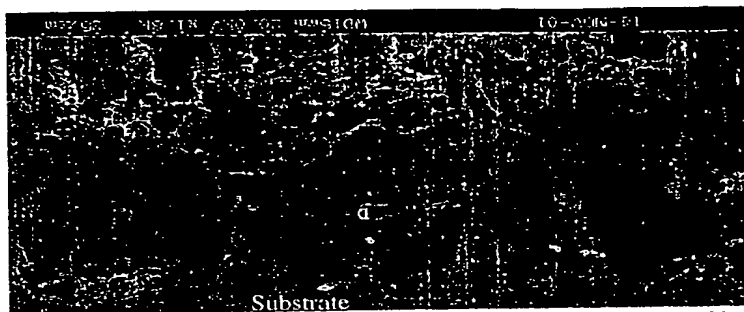


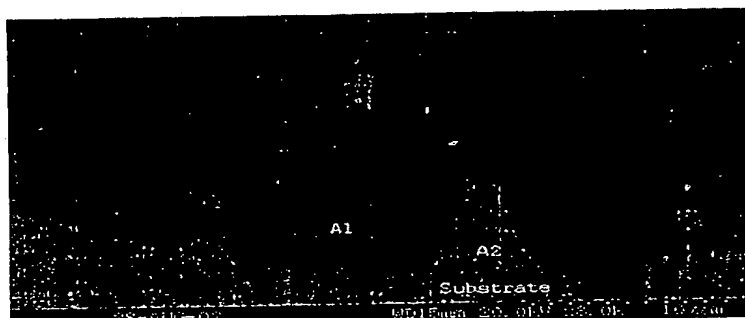
Fig. 2



(a) Bath A (x1.8k)



(b) Bath B (x1.2k)



(c) Bath C (x8k)



(d) Bath D (x10k)

Fig. 3

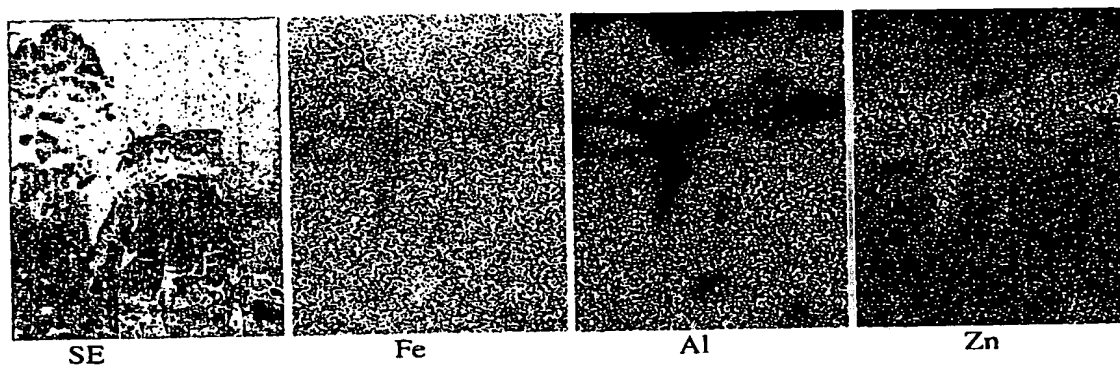


Fig. 4a

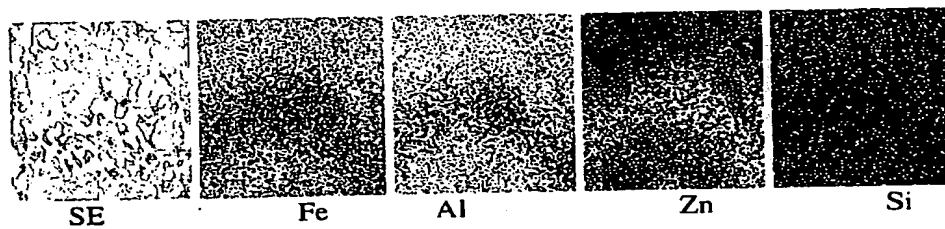


Fig. 4b

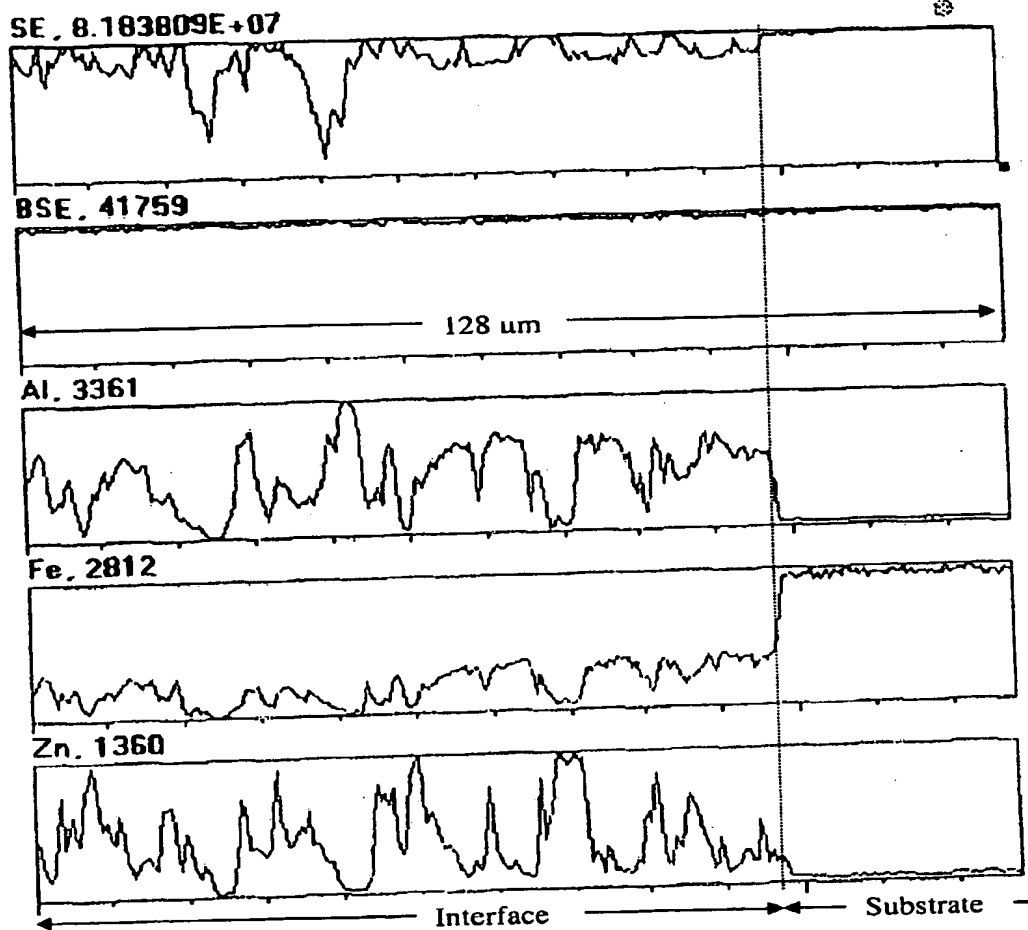


Fig. 5

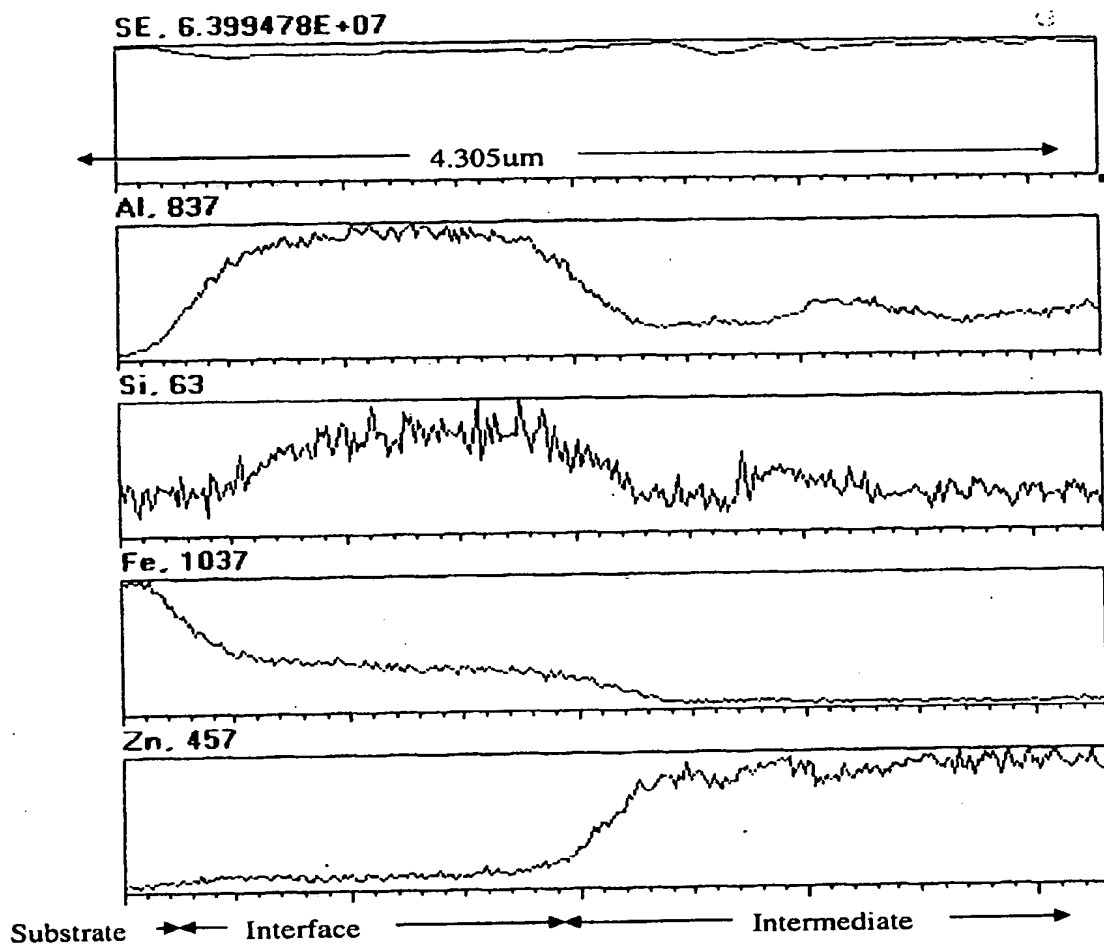


Fig. 6

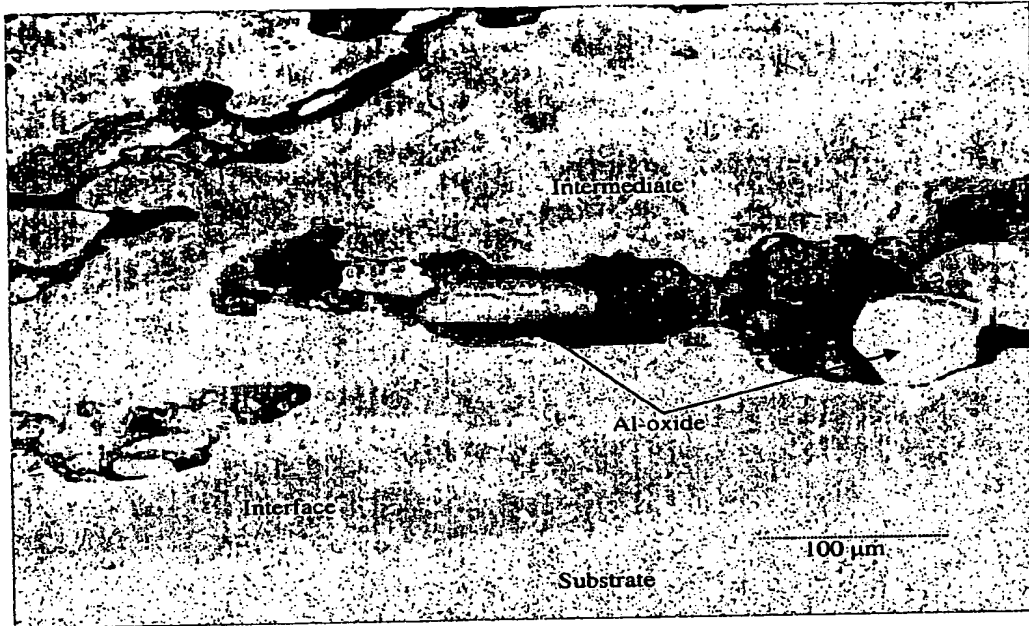


Fig. 7

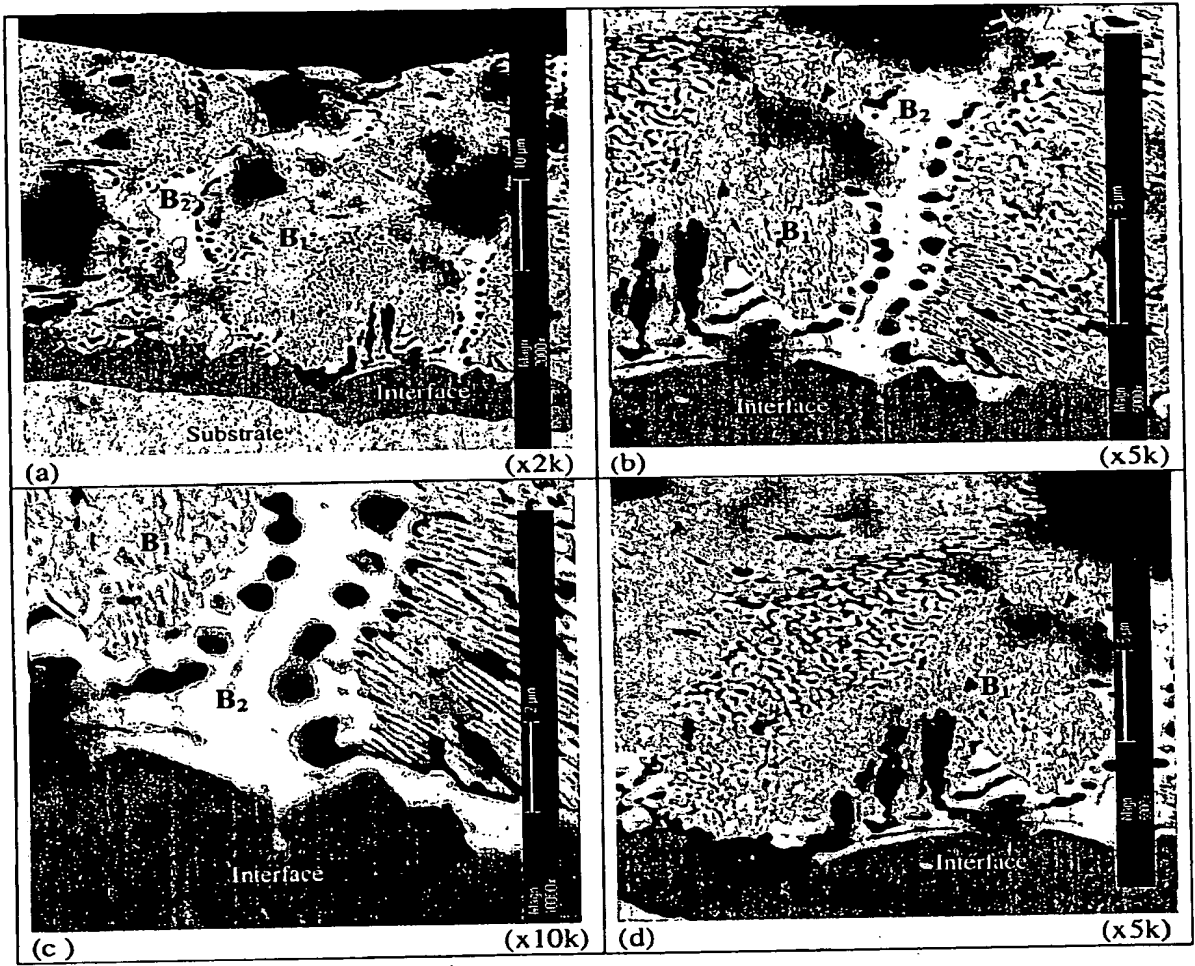


Fig. 8

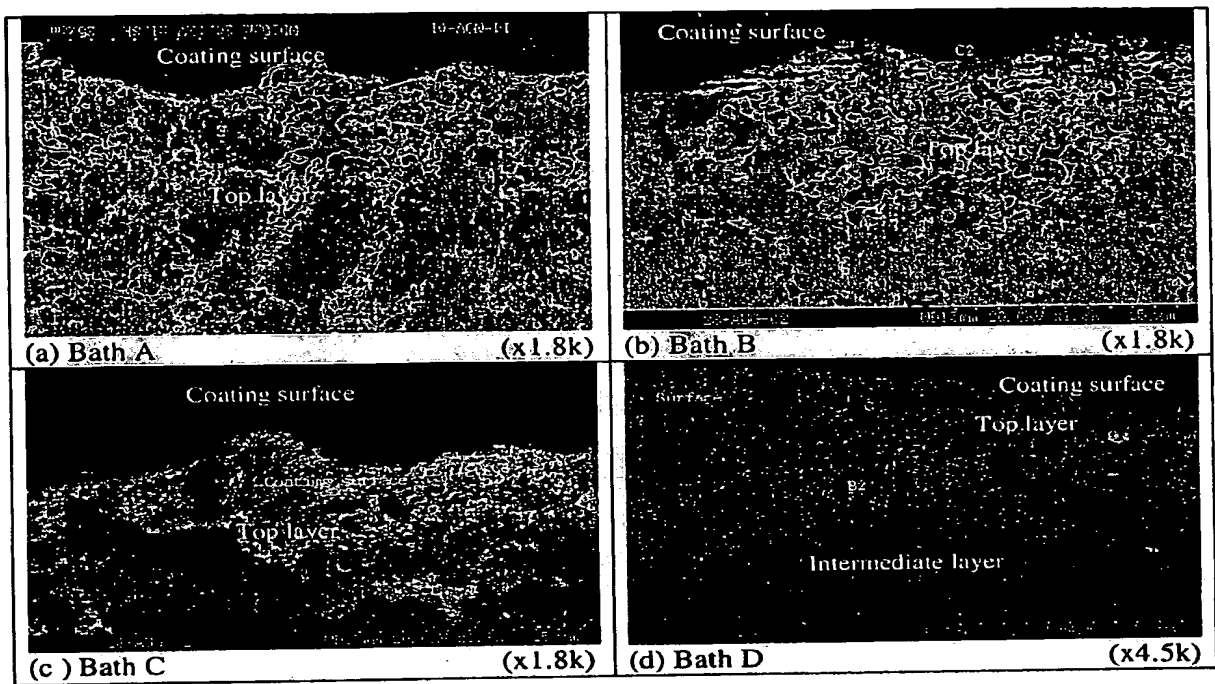


Fig. 9

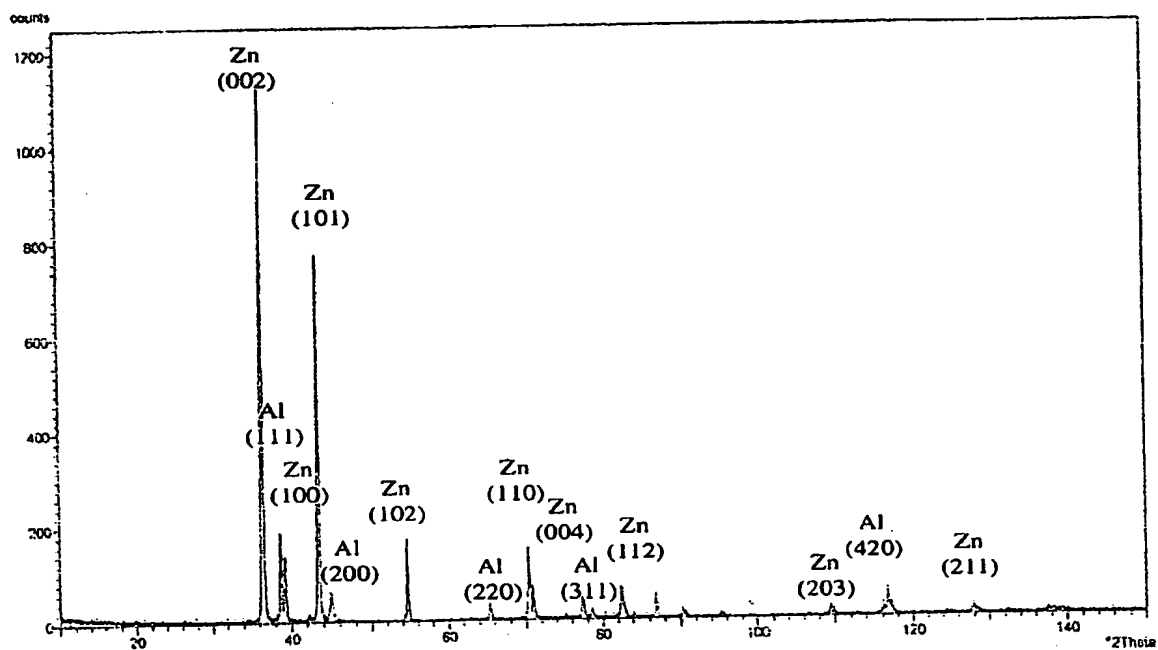


Fig. 10a

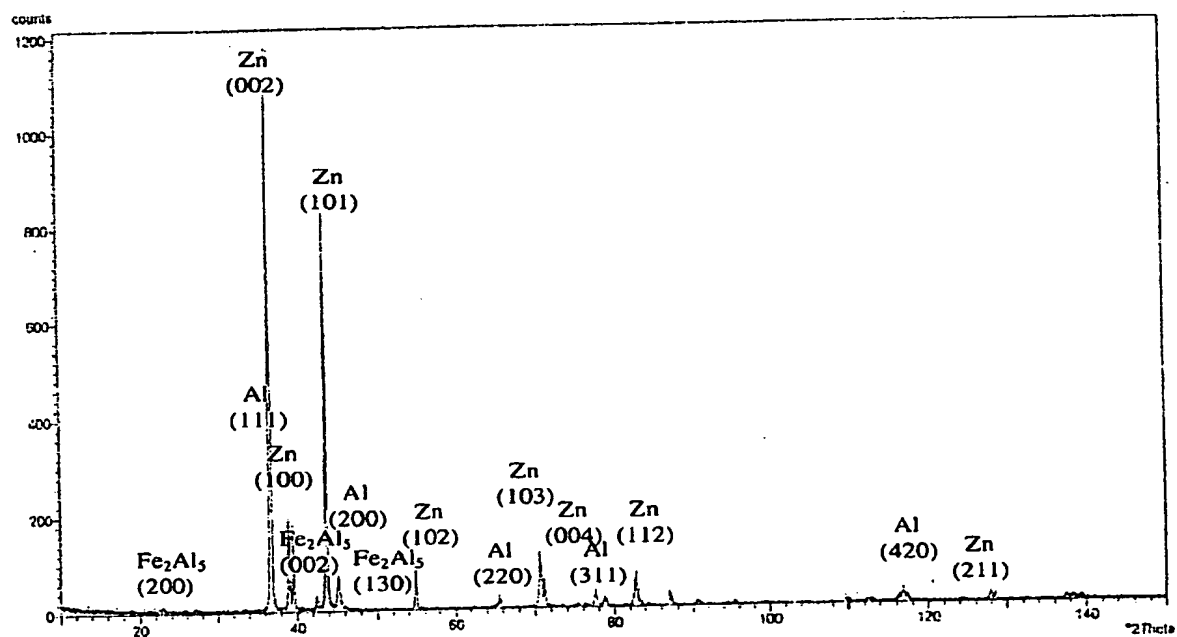


Fig. 10b

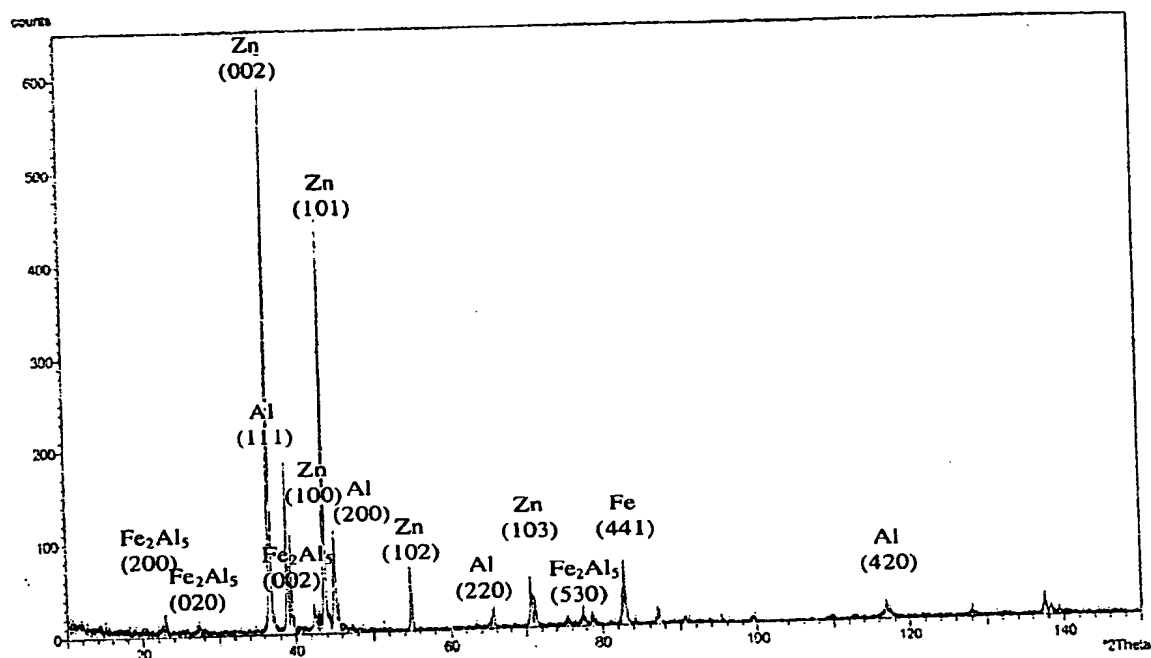


Fig. 10c

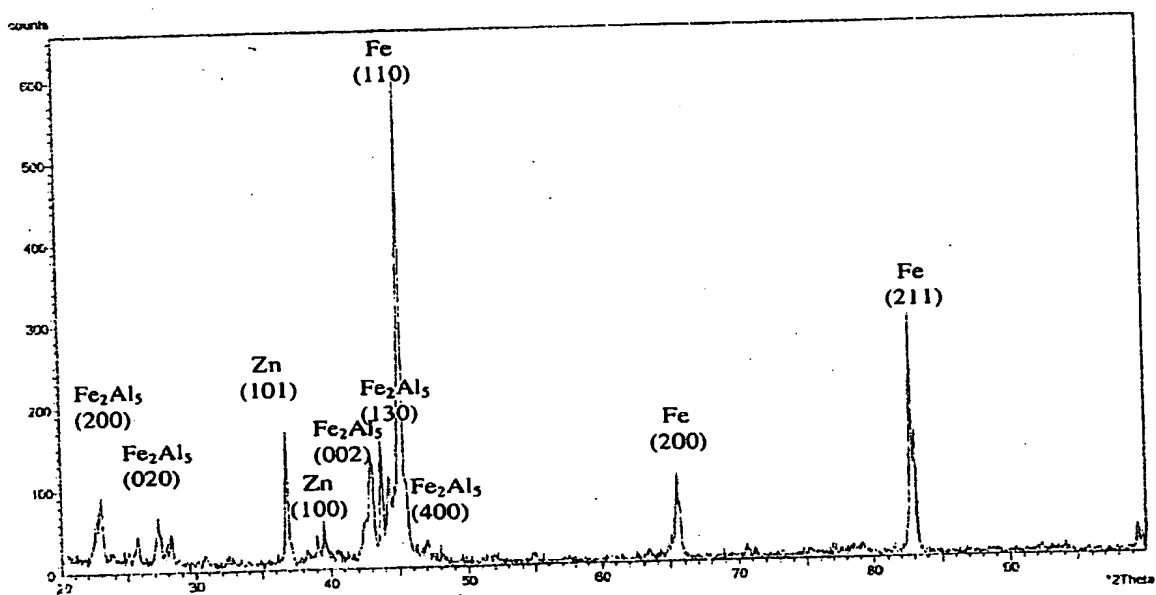


Fig. 10d

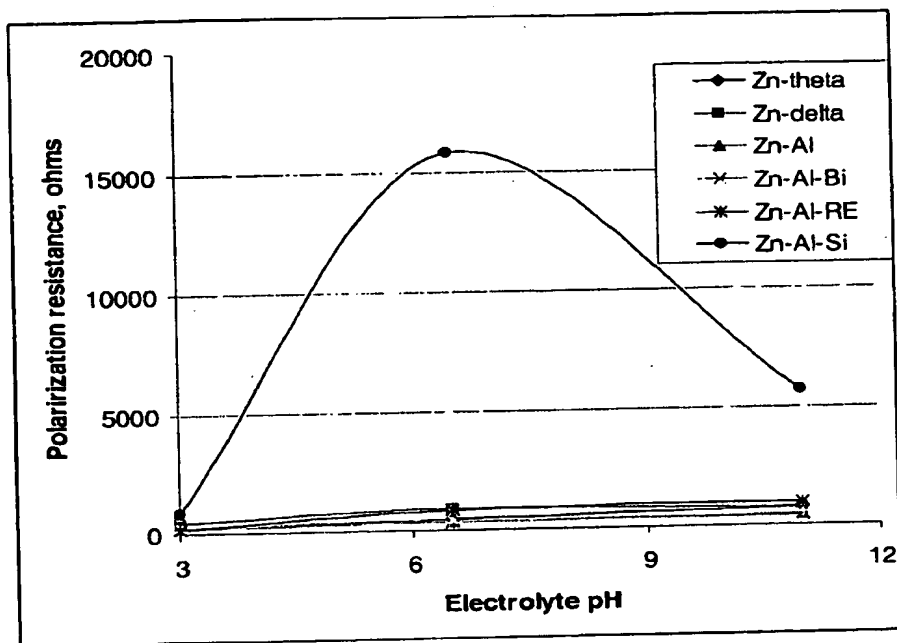


Fig. 11

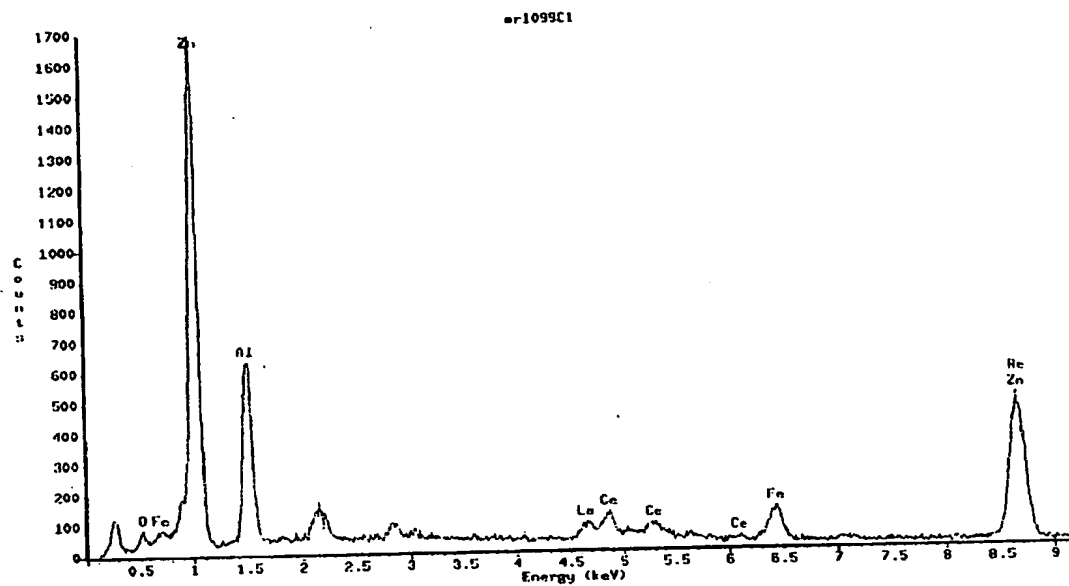


Fig. 13

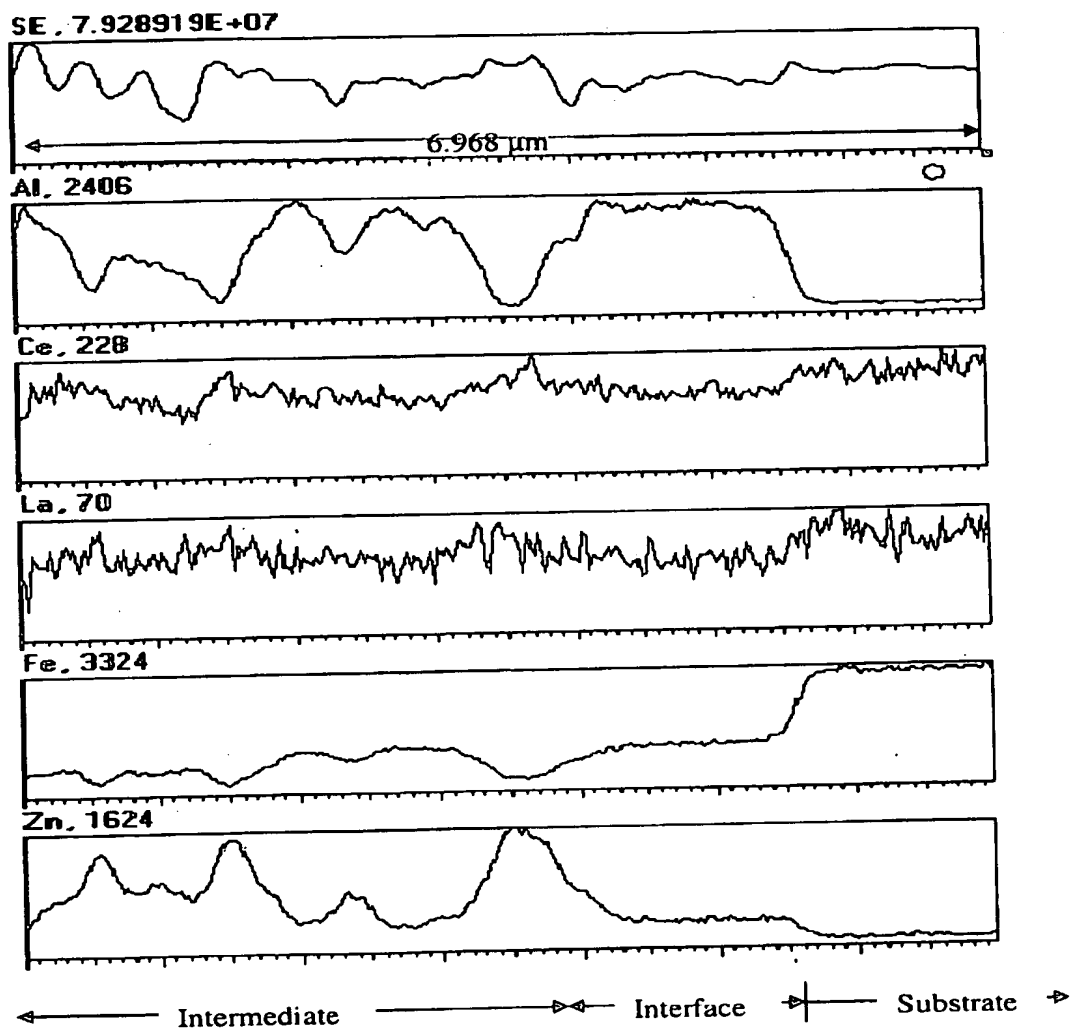


Fig. 14